PHYSICAL REVIEW A **78**, 061402(R) (2008)

Retrieving photorecombination cross sections of atoms from high-order harmonic spectra

Shinichirou Minemoto,[1,*] Toshihito Umegaki,[2] Yuichiro Oguchi,[1] Toru Morishita,[2,3,†] Anh-Thu Le,[4] Shinichi Watanabe,[2] and Hirofumi Sakai[1]

[1]*Department of Physics, Graduate School of Science, The University of Tokyo, 7-3-1 Hongo, Bunkyo-ku, Tokyo 113-0033, Japan*

[2]*Department of Applied Physics and Chemistry, University of Electro-Communications, 1-5-1 Chofu-ga-oka, Chofu-shi, Tokyo 182-8585, Japan*

[3]*PRESTO, Japan Science and Technology Agency, Kawaguchi-shi, Saitama 332-0012, Japan*

[4]*Department of Physics, Cardwell Hall, Kansas State University, Manhattan, Kansas 66506, USA*

(Received 23 October 2008; published 16 December 2008)

We observe high-order harmonic spectra generated from a thin atomic medium, Ar, Kr, and Xe, by intense 800-nm and 1300-nm femtosecond pulses. A clear signature of a single-atom response is observed in the harmonic spectra. Especially in the case of Ar, a Cooper minimum, reflecting the electronic structure of the atom, is observed in the harmonic spectra. We successfully extract the photorecombination cross sections of the atoms in the field-free condition with the help of an accurate recolliding electron wave packet. The present protocol paves the way for exploring ultrafast imaging of molecular dynamics with attosecond resolution.

DOI: 10.1103/PhysRevA.78.061402 PACS number(s): 32.80.Rm, 42.65.Ky, 42.50.Hz

When an intense femtosecond pulse interacts with an atom or a molecule, the electron freed by tunnel ionization is driven by the laser's electric field so as to return to the vicinity of the ionic core, and collides with the core. The "recollision" process provides various phenomena including high-order harmonic generation [1], elastic scattering [2], and inelastic excitation or ionization [3]. Since tunnel ionization and recollision occur within one optical cycle of a visible or infrared laser pulse, ultrafast dynamics as short as a few hundreds of attoseconds can be examined through the recollision processes [4,5].

Among the varieties of recollision physics, high-order harmonic generation is the first to be utilized for tomographic imaging of molecular orbitals [6,7] and for ultrafast nuclear dynamics [8,9]. High-order harmonics are generated by the transition from the continuum to the ground bound state. In order to investigate the instantaneous images or dynamics of the bound state, one needs to have accurate information about the recolliding wave packet. So far, the recolliding wave packet has been analyzed assuming a plane wave, which may not be a good approximation, especially for the low-energy (<1 keV) transitions.

Recently, Morishita *et al.* have formulated the recolliding electron wave packet accurately by solving the time-dependent Schrödinger equation directly [10,11]. The accuracy of the wave packet has been experimentally tested by observing the angular distributions of the backscattered electrons from atoms with femtosecond pulses [12,13]. Using an accurate recolliding wave packet, tomographic imaging and ultrafast dynamics can be investigated from high-order harmonics. In this Rapid Communication, we observe high-order harmonic spectra generated from Ar, Kr, and Xe atoms, and extract photorecombination cross sections based on the accurate recolliding wave packet. Experiments are performed by using fundamental pulses with two different wavelengths. The results are compared with each other and with the theoretical differential photorecombination (the inverse process of photoionization) cross sections.

The details of the experimental setup will be described elsewhere [14]. Briefly, an intense, femtosecond laser pulse is focused into a pulsed gas jet in the vacuum with a 400-mm-focal-length lens. As fundamental pulses, we use the output from a Ti:sapphire (TiS) amplification system (wavelength $\lambda_{\mathrm{TiS}} \sim 800$ nm) or that from an optical parametric amplifier (OPA; $\lambda_{\mathrm{OPA}} \sim 1300$ nm) pumped by the TiS pulse. The pulse widths are measured by a single-shot autocorrelator and are found to be ~ 50 and ~ 60 fs for the TiS and the OPA pulses, respectively. The resulting xuv radiation is spectrally dispersed by an xuv spectrometer and is recorded by a charge-coupled-device (CCD) camera.

The wavelength dependence of harmonic intensities is corrected by considering the transmittance of the 150-nm-thick Al xuv filter, the reflection efficiency of the Au-coated grating, and the quantum efficiency of the CCD camera. The grating efficiency is calculated from the reflectance data of Au [15], and the CCD efficiency is obtained from the manufacturer's data. The transmittance of the Al xuv filter is evaluated by using the OPA output as the fundamental pulse. Since our CCD is insensitive to the 1300-nm fundamental pulses, the harmonic intensities can be directly compared with and without the xuv filter.

In the experiments, we make every effort to ensure that the observed high-order harmonic spectra are dominated by the single-atom response and that the propagation effects are minimized [16]. Some of the causes by which the observed harmonic spectra deviate from the single-atom response include self-phase-modulation of the fundamental pulse, ionization (depletion) of the atomic medium and subsequent production of free electrons, absorption of the harmonics by the medium, and phase mismatch between the harmonic and the fundamental field. To minimize these effects and extract the single-atom response from the high-order harmonic spectra, we employ a pulsed supersonic valve, which can supply a thin pulsed gas in the interaction region.

*minemoto@phys.s.u-tokyo.ac.jp

†toru@pc.uec.ac.jp

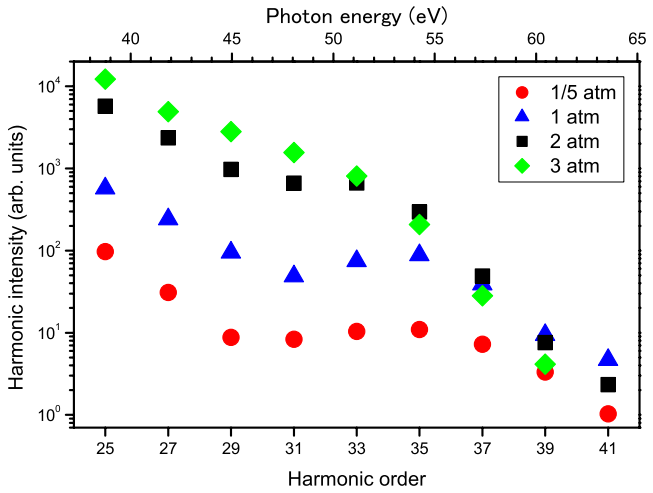

FIG. 1. (Color online) Typical harmonic spectra observed by the TiS pulses for the Ar gas pressures of 3 (green diamonds), 2 (black squares), 1 (blue triangles), and 1/5 atm (red circles).

Figure 1 shows typical harmonic spectra with the TiS pulses for various backing pressures of Ar gas. A variation of the backing pressure leads to a change in the atomic density in the interaction region. The accuracy of the backing pressure is maintained within $\pm 10^{-2}$ atm by monitoring a pressure gauge. In our experimental system, the atomic density ρ is estimated to be $\sim 2 \times 10^{17}/\mathrm{cm}^3$ when the backing pressure of 1 atm is used. At this atomic density and a typical ionization cross section σ of 5×10^{-18} cm^2 at 40 eV [17], the absorption length $L_{\mathrm{abs}} = 1/(\sigma\rho)$ is 10 mm, which is much longer than the medium length $L_{\mathrm{med}} \sim 1$ mm. We find that, below 2 atm, there appears a minimum between the 25th and 35th harmonics. The observed minimum is a signature of the electronic structure of the Ar atom and the main topic of this Rapid Communication as discussed below. In order to decrease the atomic density as much as possible, the timing of the opening of the pulsed valve is adjusted, keeping the backing pressure at 1 atm, so that a thin front part of the gas jet interacts with the femtosecond pulses. The atomic density is then estimated to be $\sim 1/5$ of that at the peak of the gas jet by comparing the produced ion intensities. We refer to this condition as the 1/5 atm condition. The red circles show the harmonic spectra in the 1/5 atm condition. The overall structure is almost identical to that at 1 atm (blue triangles) except for the decreased intensity of the harmonics. On the other hand, when the backing pressure is increased to 2 atm (black squares), the minimum around the 30th-order harmonic still appears but becomes unclear compared to that below 1 atm. When the backing pressure is further increased to 3 atm (green diamonds), the harmonic intensity decreases monotonically with increasing harmonic order, and the highest-order harmonic observed (cutoff order) is the 39th. The reduced cutoff order is due either to the production of free electrons or to the self-phase modulation (defocusing) of the fundamental pulse.

Another issue to be examined to ensure the single-atom response is the phase matching condition, i.e., the position of the focus with respect to the gas medium and the position of the detector with respect to the far-field pattern of the harmonics. The harmonic spectra in Fig. 1 are observed in the condition that the focus is in the middle of the gas jet and the entrance slit of the spectrometer is located in the (far-field) center of the harmonics. In this arrangement, the observed harmonics correspond mainly to those from the short trajectories [18]. At the lowest atomic density of the 1/5 atm condition, we confirm that the harmonic spectra are almost identical even when the position of the focus is changed. On the other hand, when the focus is located ~ 1 mm before the gas jet in the 1 atm condition, the spectral shape approaches that at 2 atm shown in Fig. 1, probably due to the saturation effects, when the generation of the harmonics and the absorption by the gas medium are balanced with each other [19]. Therefore, we set the gas pressure to the 1/5 atm condition and focus the laser beam at the center of the gas jet to ensure the experimental condition where the single-atom response is dominant in the high-order harmonic spectra.

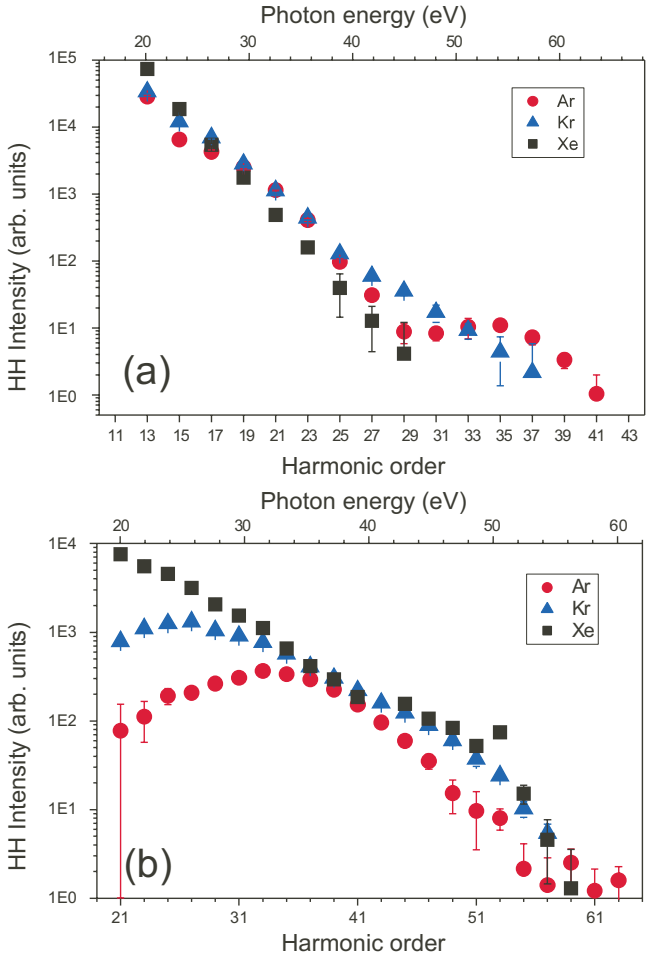

FIG. 2. (Color online) Harmonic spectra observed for Ar (red circles), Kr (blue triangles), and Xe (black squares) with (a) the TiS and (b) the OPA pulses.

Figure 2(a) shows the harmonic spectra generated from Ar (red circles), Kr (blue triangles), and Xe (black squares) by the TiS pulses. The cutoff orders of harmonics are found to be 41st (Ar) and 37th (Kr), which give the effective peak intensities of $\sim 2 \times 10^{14}$ W/cm^2 from the well-known cutoff formula. The cutoff order of the 29th for Xe gives a lower effective intensity, which may be attributed to the depletion

of the ground state resulting from the lower ionization potential. Since the peak intensity of 2×10^{14} W/cm^2 is well above the saturation intensity for Xe with the ionization potential of 12 eV, the neutral atoms are depleted before the pulse reaches the peak intensity and the measured harmonic spectra are regarded as those at the "effective" peak intensity. In the spectra for Kr and Xe, the harmonic intensities decrease monotonically as the harmonic order increases. The spectrum for Ar, however, has a clear minimum at around the 31st-order harmonics (~48 eV). The minimum at ~50 eV has also been observed in photoabsorption (the inverse process of photorecombination) spectra of Ar [17]; it is known as the Cooper minimum. In the low-energy region of Ar, the dipole transitions are dominated by those from the outermost $3p$ orbitals to both s and d continuum states. At around the Cooper minimum, the dipole moment of the d waves changes its sign, so that the photorecombination (photoabsorption) cross section is reduced. Although the Cooper minimum has been observed also in Kr (~70 eV) and Xe (~200 eV) for the inner orbitals [17], those photon energies lie beyond the present measurements.

As shown above, in the high-order harmonic spectra is embedded information about the electronic structure of atoms, just as in photoabsorption spectra. In order to quantitatively discuss the electronic structures, we need to extract the photorecombination cross sections (PRCSs) from the measured harmonic spectra. For this purpose, we follow the procedure proposed by Morishita *et al.* [10]. In Ref. [10], the high-order harmonic spectra $S(\omega)$ can be expressed as $S(\omega)=W(E)\sigma(\omega)$, where $\sigma(\omega)$ is the PRCS and the prefactor $W(E)$ is the recolliding electron wave packet. Here the kinetic energy E of the electron is related to the photon energy as $\hbar\omega=E+I_p$ with I_p the ionization potential. The electron wave packet is calculated numerically by solving the time-dependent Schrödinger equation [20] for the scaled H atom whose I_p corresponds to the target atom. The measured harmonic intensity is divided by the calculated wave packet at each harmonic order, yielding the PRCS.

The green circles in Fig. 3 show the PRCSs thus extracted for (a) Ar, (b) Kr, and (c) Xe. The red curves show the theoretical PRCSs calculated from a one-electron model potential (see Ref. [21]). We use the form of the effective potential in Refs. [22,23] for Ar and that in Ref. [24] for Kr and Xe. In the case of Ar [Fig. 3(a)], one can see that the extracted PRCSs agree reasonably with the theoretical ones not only around the Cooper minimum (~50 eV) but also in the whole photon energy range from 25 to 65 eV. Furthermore, in the Kr and Xe cases [Figs. 3(b) and 3(c)], the agreements between the extracted and the theoretical cross sections are fairly good within the experimental uncertainties.

In order to further test the validity of the present methodology, we use the OPA pulses instead of the TiS pulses and measure the harmonic spectra. Figure 2(b) shows the harmonic spectra generated by the OPA pulses. In order to observe the spectra, the backing pressure needs to be increased to 2 atm to compensate for the low harmonic intensity, which is caused partly because of the lower peak intensity (~1/3) compared to the TiS pulses and partly because of the lower efficiency of harmonic generation with a longer-wavelength pulse [25,26]. When comparing the results with the OPA pulses to those with the TiS pulses, we find that the harmonic spectra retain the single-atom responses at least in the photon energy range higher than 35 eV (37th-order harmonic for the OPA pulse) in spite of rather high atomic densities. The successful observations of single-atom responses with higher atomic densities may come from the fact that the smaller

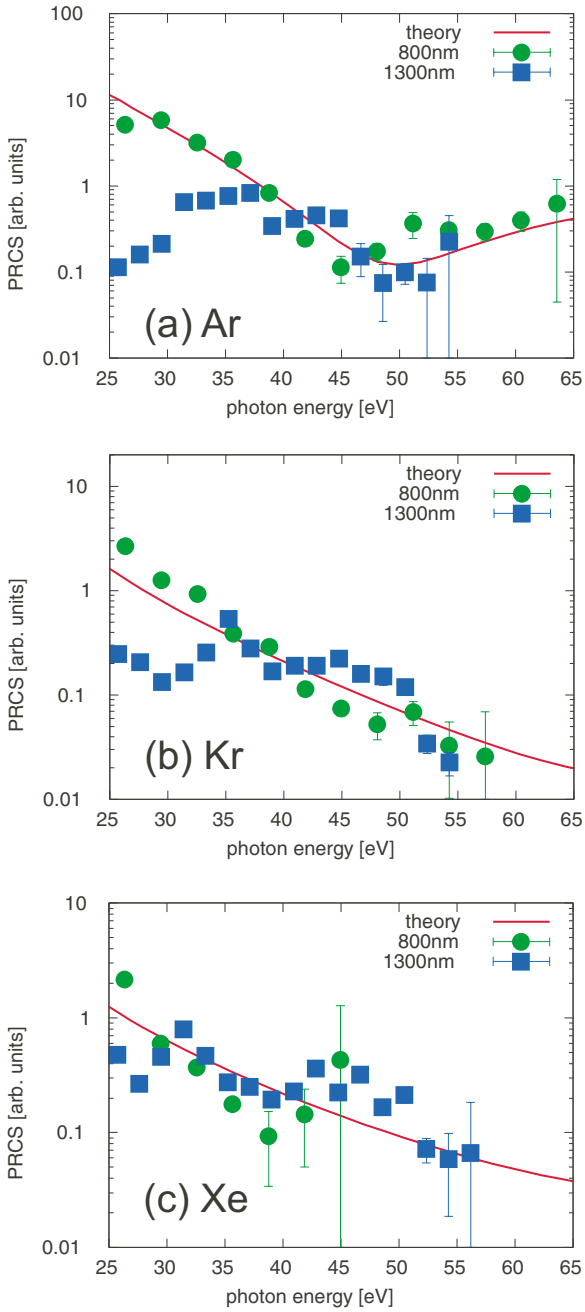

FIG. 3. (Color online) Extracted photorecombination (the inverse of photoionization) cross sections (PRCSs) of (a) Ar, (b) Kr, and (c) Xe. The green circles and blue squares represent the cross sections extracted from the harmonic spectra with the TiS and the OPA pulses, respectively. The "effective" intensities of 2.1, 2.2, and 1.3×10^{14} W/cm^2 are used for Ar, Kr, and Xe, respectively, with the TiS pulses, and those of 6.3, 7.7, and 7.6×10^{13} W/cm^2 are used with the OPA pulses. The red curves show the theoretical PRCSs.

photon energy of the OPA pulse as well as its lower intensity ($\sim 7\times 10^{13}$ W/cm^2) have led to the suppression of ionization and self-phase-modulation, both of which will induce strong propagation effects. As in the case with the TiS pulses, the spectrum of Ar shows a rapid decrease at around the 50th-order harmonic ($\sim$48 eV), which can be explained by the Cooper minimum.

With the same procedure used for the results with the TiS pulses, we retrieve PRCSs (the blue squares in Fig. 3) with the effective intensities of $\sim 7\times 10^{13}$ W/cm^2. Looking at the photon energy range higher than 35 eV, the extracted PRCSs are consistent with those extracted from the harmonic spectra by the TiS pulses and the theoretical ones. At photon energies lower than 30 eV, however, the cross sections obtained by the OPA pulses deviate from those by the TiS pulses most probably due to the absorption by the medium. In this low-energy region, the photoabsorption cross sections of all the target atoms (Ar, Kr, and Xe) exceed 10^{-17} cm^2 [17] and the absorption length L_{abs} is 2.5 mm or less, which is close to the medium length $L_{\mathrm{med}}\sim 1$ mm. Such a strong reabsorption of the generated harmonics hinders the observation of single-atom response and makes the retrieved PRCSs smaller than the accurate ones.

In conclusion, the photorecombination cross sections of the target ion with a freed electron can be retrieved from the observed high-order harmonic spectra by using the procedure in Ref. [10]. The retrieved cross sections are independent of the wavelength of the fundamental pulses, and they agree well with the theoretical cross sections. The biggest advantage of the present methodology for ultrafast dynamic studies is that the method can provide information on the electronic structure in the field-free condition because the recollision takes place around 2/3 of an optical cycle after tunnel ionization when the electric field is almost zero. With the help of state-of-the-art molecular orbital calculations, one could obtain the most probable instantaneous geometric structure of a molecule which reproduces the photorecombination cross sections retrieved through the present method. When we change the wavelength of the fundamental pulse and consequently the recollision time [27], the ultrafast nuclear dynamics can be traced with a time resolution as fast as a hundred attoseconds. Furthermore, when we use aligned [28] or oriented molecules [29] and follow the present protocol, the door opens for investigating ultrafast electronic stereodynamics [30], without any reference to or assumption about the system.

This work was financially supported by Grants-in-Aid No. 19204041 and No. 19540416 from the Japan Society for the Promotion of Science (JSPS), by the PRESTO program of the Japan Science and Technology Agency (JST), and by the JSPS Bilateral joint program between the U.S. and Japan.

[1] For a recent review, see J. G. Eden, Prog. Quantum Electron. **28**, 197 (2004), and references therein.
[2] G. G. Paulus, W. Nicklich, H. Xu, P. Lambropoulos, and H. Walther, Phys. Rev. Lett. **72**, 2851 (1994).
[3] H. Niikura *et al.*, Nature (London) **417**, 917 (2002).
[4] P. B. Corkum and F. Krausz, Nat. Phys. **3**, 381 (2007).
[5] R. Tores and J. P. Marangos, J. Mod. Opt. **54**, 1883 (2007).
[6] J. Itatani *et al.*, Nature (London) **432**, 867 (2004).
[7] T. Kanai, S. Minemoto, and H. Sakai, Nature (London) **435**, 470 (2005).
[8] M. Lein, Phys. Rev. Lett. **94**, 053004 (2005).
[9] S. Baker *et al.*, Science **312**, 424 (2006).
[10] T. Morishita, A.-T. Le, Z. Chen, and C. D. Lin, Phys. Rev. Lett. **100**, 013903 (2008).
[11] A.-T. Le, T. Morishita, and C. D. Lin, Phys. Rev. A **78**, 023814 (2008).
[12] M. Okunishi, T. Morishita, G. Prümper, K. Shimada, C. D. Lin, S. Watanabe, and K. Ueda, Phys. Rev. Lett. **100**, 143001 (2008).
[13] D. Ray, B. Ulrich, I. Bocharova, C. Maharjan, P. Ranitovic, B. Gramkow, M. Magrakvelidze, S. De, I. V. Litvinyuk, A. T. Le, T. Morishita, C. D. Lin, G. G. Paulus, and C. L. Cocke, Phys. Rev. Lett. **100**, 143002 (2008).
[14] Y. Oguchi, S. Minemoto, and H. Sakai (unpublished).
[15] J. A. Samson and D. L. Ederer, *Vacuum Ultraviolet Spectroscopy* (Academic Press, San Diego, 2000).
[16] J. Levesque, D. Zeidler, J. P. Marangos, P. B. Corkum, and D. M. Villeneuve, Phys. Rev. Lett. **98**, 183903 (2007).
[17] J. A. R. Samson and W. C. Stolte, J. Electron Spectrosc. Relat. Phenom. **123**, 265 (2002).
[18] M. Bellini *et al.*, Phys. Rev. Lett. **81**, 297 (1998).
[19] E. Constant *et al.*, Phys. Rev. Lett. **82**, 1668 (1999).
[20] T. Morishita, Z. Chen, S. Watanabe, and C. D. Lin, Phys. Rev. A **75**, 023407 (2007).
[21] U. Fano and J. W. Cooper, Rev. Mod. Phys. **40**, 441 (1968).
[22] H. G. Muller, Phys. Rev. A **60**, 1341 (1999).
[23] E. S. Toma and H. G. Muller, J. Phys. B **35**, 3435 (2002).
[24] R. H. Garvey, C. H. Jackman, and A. E. S. Green, Phys. Rev. A **12**, 1144 (1975).
[25] J. Tate *et al.*, Phys. Rev. Lett. **98**, 013901 (2007).
[26] K. Schiessl, K. L. Ishikawa, E. Persson, and J. Burgdörfer, Phys. Rev. Lett. **99**, 253903 (2007).
[27] H. Niikura *et al.*, Nature (London) **421**, 826 (2003).
[28] H. Sakai *et al.*, J. Chem. Phys. **110**, 10235 (1999).
[29] H. Sakai, S. Minemoto, H. Nanjo, H. Tanji, and T. Suzuki, Phys. Rev. Lett. **90**, 083001 (2003).
[30] D. Herschbach, Eur. Phys. J. D **38**, 3 (2006).